SLAC–PUB–6315
August 1993
(E)

INTERACTION REGION ISSUES AT THE NLC*

THOMAS W. MARKIEWICZ
Stanford Linear Accelerator Center
Stanford University , Stanford, CA 94309, USA

1. Introduction

The SLAC-based NLC working group[1] has been considering issues relevant to the operation of an X-band 0.5–1.0 TeV collider. This report summarizes some of the results the group has achieved to date.

The NLC[2] will collide trains of closely spaced bunches of 10^{10} particles. Typical parameters are 1.4 ns for the inter-bunch spacing, 100 bunches/train, and 180 trains/sec. Its final focus (FF) will provide spot sizes at the interaction point (IP) of dimensions σ_x = 300–400 nm, σ_y = 2–3 nm, and σ_z = 100 μm. The closely spaced bunches and the desire to have each bunch interact only with its partner imply that there must be a crossing angle at the IP. The high charge density will cause backgrounds due to electromagnetic beam-beam interactions and particle detectors with good timing resolution will be required to separate hits from the interaction causing the trigger from the background hits arising from other bunches in the train. The 2 nm beam spots will challenge experimenters to get and keep the beams in collision. They will require special consideration to be given to issues of alignment, ground motion, and vibrations induced by the transfer of cooling fluids. The detector masking must be able to reduce to manageable levels the backgrounds due to synchrotron radiation in the final quadrupoles and to the beam-beam interaction. Simulations of these backgrounds should consider the worst case of 2 beam trains of 10^{12} particles each at 500 GeV.

2. The Interaction Region

There are many potential ways to attack the problems listed above. The approach we have taken is to make some, perhaps arbitrary, choices for now and to bootstrap our way into a full investigation of the optimal detector and interaction region. Figures 1 and 2 show the current conception of the beamline at the IP. There is a 40 mrad crossing angle. The FF quadrupole doublet is composed of Sm_2Co_{17} permanent magnets in order to avoid the vibrations that cooling fluids would produce in conventional or superconducting magnets. The magnet diameter is 8 cm, its aperture 1 cm, and it extends to 1.5 m from the IP. The cross sectional cut at 1.5 m indicates the 6 cm separation of the exit beam from the incoming beam. These magnets are solidly supported in the ground with rigid mounts to ensure the long term stability of the alignment. This choice couples ground vibrations directly to the system and will require schemes to reduce its effect. To enhance the coherence of the system, both ends of the FF are tied together with a 1 cm

* Work supported by Department of Energy contract DE-AC03-76SF00515.

Contributed to the 2nd International Workshop on Physics and Experiments With Linear e^+e^- Colliders, Waikoloa, HI April 26–30, 1993.

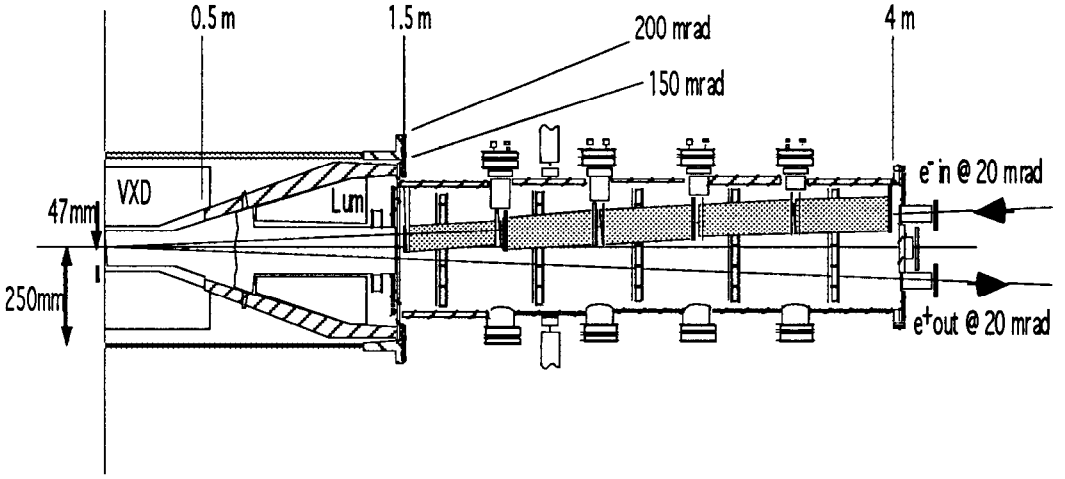

Figure 1. Plan view of the IR region. Vertical scale is 2x horizontal scale.

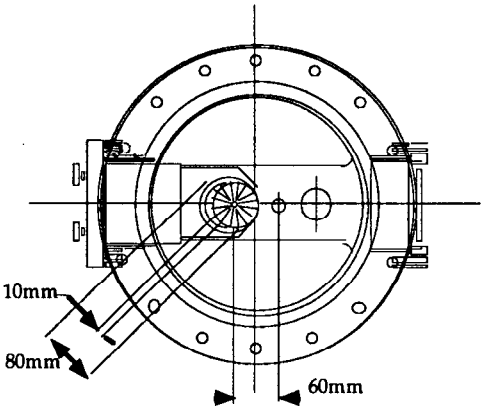

Figure 2. Cross section of the beam pipe at z = 1.5 m.

thick carbon fiber/foam composite (0.5% r.l.) support tube at 25 cm radius. There is a conical tungsten mask from 0.5–1.5m in z covering the polar angle region of 150/200 mrad. The luminosity monitor resides within this angular region. A presumably CCD-based vertex detector resides in the area between the 5.0 cm radius beampipe and the support tube. Current simulations consider a standard cylindrical gas drift chamber as the tracking detector between 25 cm and 1 m.

These choices have led to the following experimental program. To understand the magnitude of the problem and to gain experience with the relevant techniques, we have made measurements of the vibrations of a simplified support tube. We have considered SLC-inspired schemes to reduce the effect of vibration by using fast feedback. We have designed and are prototyping a scheme to magnetically stabilize the FF quads using feedback from an inertially suspended pickup loop. We report on the results of synchrotron radiation calculations for the current lattice and EGS modeling of the detector masking. EGS / GEANT modeling of beam-beam interactions using the ABEL code is reported elsewhere.[3] Finally, we update our calculations of the expected muon background.

3. Final Focus Quad Vibrations

3.1. Vibration measurements

Vibrations of a rigidly mounted final focus system will be due to ground motion, amplified at the natural frequencies of the FF support structure, and to whatever moving parts may be found at the experiment: pumps, compressors, etc. Geophysicists have long made measurements of the rms amplitude of ground motion as a function of frequency. The rms amplitude per frequency interval falls very rapidly from zero frequency to 0.05 Hz. A typical rms displacement is 100 nm for the frequency range from 0.001 to 0.01 Hz. At the NLC we will need to stabilize the beams at the 1 nm level. The large wavelengths at these frequencies relative to the separation of the FF quads lessen the importance of these large displacements. At very large frequencies, on the other hand, there is essentially no displacement. The frequency range of interest is that between, say 0.02 Hz or so and about 100 Hz.

To gain familiarity with the measurement techniques and a first hand feeling for the magnitude of the problem, we have made vibration measurements on an idealized support tube. The structure itself is a 10 m long, 30 cm diameter, 2.5 cm wall aluminum tube supported on the floor by metal V blocks at ±2.85 m. This length is similar to that which would be required to contain both sides of the final focus permanent quad magnets. Finite element analysis of this structure gives its normal modes as 20, 47, 70, and 125 Hz, the exact number depending on the details of its support. The test was carried out in the SLD experimental pit at the SLC. Two seismometers were placed symmetrically about the midpoint at ±1.22 m and their signals added or subtracted to find the symmetric and asymmetric components of the tube's vibrations. As the asymmetric mode will cause one side of the FF to point up and the other down, it is the more important.

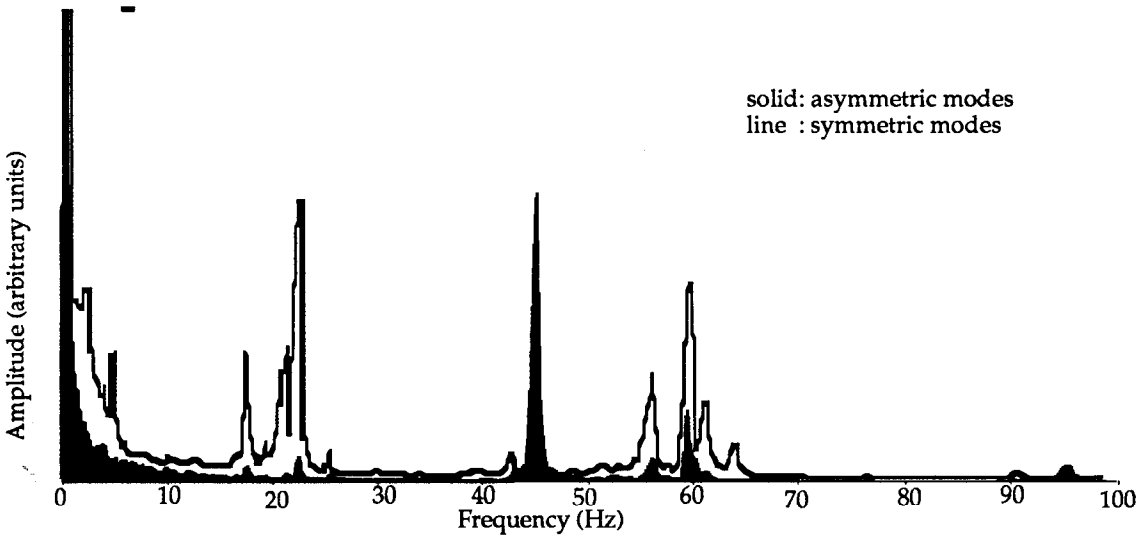

Figure 3. Displacement of a model FF support tube as a function of frequency.

Figure 3 presents the results of these measurements, where the vertical scale is linear and arbitrary. Integrating the (open) symmetric histogram from 3 Hz, the lower limit of the seismometer's sensitivity, to 100 Hz, one finds 29 nm of rms displacement, almost all due to the resonant structures at 22 Hz (19 nm) and 60 Hz (16 nm). The multi-peak structures are probably due to slightly different frequencies for vertical and lateral vibration. In the asymmetric (filled) histogram the total is 19 nm, 18 nm of which is due to the resonance at 44 Hz. The next mode, at 95 Hz, contributes but 1.6 nm, while the structure at 59 Hz, driven by a water pump in the hall, contributes 5 nm. These vibrations then will need to be dealt with through external means if the NLC beams are to be stable to 1 nm.

3.2. Fast feedback

One of the reasons for the dramatic improvement in SLC uptime in 1992 and 1993 has been the implementation of many fast feedback[4] loops. These use a beam detection element, typically a beam position monitor (BPM), to drive a correcting element. In the SLC scheme the loops are microprocessor driven; they incorporate the signal from upstream loops to avoid overcorrection and transmit their correction to loops further downstream. Currently each difference signal that a given loop tries to null is averaged for 6 of the 120 Hz machine pulses. This, together with the BPM resolution and beam jitter, set the frequency dependence of the transient suppression that can be

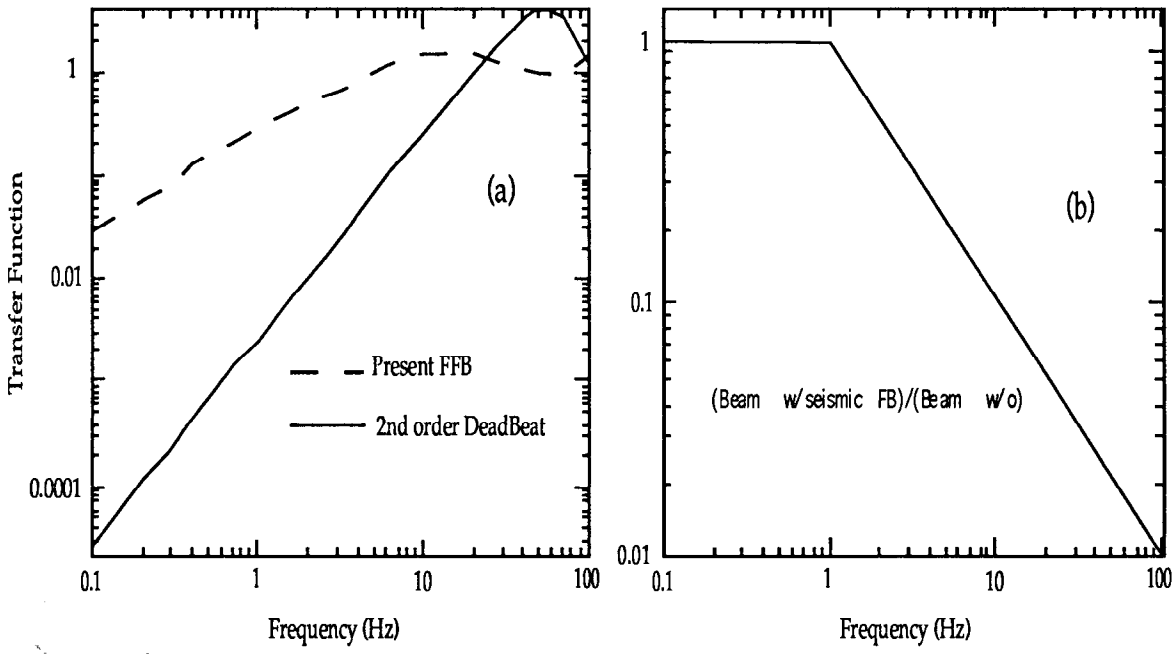

Figure 4. Part(a) gives the suppression factors for transient effects expected for a NLC fastfeedback loop. Part(b) shows the suppression factor expected from the field stabilization due to an inertially suspended pickup coil having a cutoff frequency of 1 Hz.

achieved. Such feedback is clearly more effective at low frequencies, where low is relative to the machine pulse rate; the challenge is to make the suppression more effective at higher frequencies.

In Fig. 4a the dashed curve shows the suppression factor achieved for the SLC extrapolated to the 180 Hz operating frequency of the NLC. The 6 pulse averaging provides stability at higher frequencies at the expense of better low frequency suppression. The solid curve is the transfer function expected if the difference between the difference signal on successive machine pulses is used to predict the corrector setting on the third pulse, a so-called second order deadbeat correction scheme. This is 10–100 times more effective in the 1–10 Hz range at the expense of frequencies above 20 Hz. It is presented only as an example of the type of game that may be played to tune the system to help the most troublesome frequencies.

3.3 Local Stabilization of the Magnetic Field

A potential means of stabilizing the beam at higher frequencies comes from the fact that it is only the field seen by the beam that must be constant, not the position of the magnet producing the field. In a 16-block Sm_2Co_{17} quad, the field is given by $B(r) = k(1-r1/r2)r/r2$. $B(r1) = 1.72$ Tesla for $r1 = 5$ mm and $r2 = 40$ mm, and the field gradient is constant and equal to 3.44 Tesla/cm. A 1 nm seismic movement of the magnet from its centerline then induces a 3.44 milliGauss field on the beam.

If a pickup coil can be suspended in, but inertially independent of, the bore of the magnet, a voltage will be induced in it that can then in turn be used to drive a set of compensating corrector coils wound around the exterior of the magnet. This arrangement is represented in Fig. 5. The voltage induced in a loop of area A by a dispacement of δx is given by:

$$V = \frac{d\Phi}{dt} = A\frac{dB}{dx}\frac{dx}{dt}, \qquad A = ndL; x = \delta x \sin \omega t \tag{1}$$

For a 1 cm diameter, 2.5-m-long coil of 150 turns, we expect an 8 μV signal for a 1 nm displacement at 1 Hz with a signal to noise ratio of 100:1. This is easily achievable and quite consistent with the signals delivered by commercial seismometers.

The drive requirements are also rather modest. The corrector signal would be integrated in a nulling circuit and drive a current buffer. A 50 turn coil at $r2$ would then require a current of

$$I = \frac{2r_2 G\delta x}{\mu_0 N_D} = 0.4 amps\ , \tag{2}$$

which would imply a 2 Volt supply driving 5 ohms.

The challenge here is to make a pickup coil support inertial even at very low frequencies. Figure 4b shows the expected suppression from such an arrangement assuming a suspension has a cutoff frequency of 1 Hz. We are currently constructing a

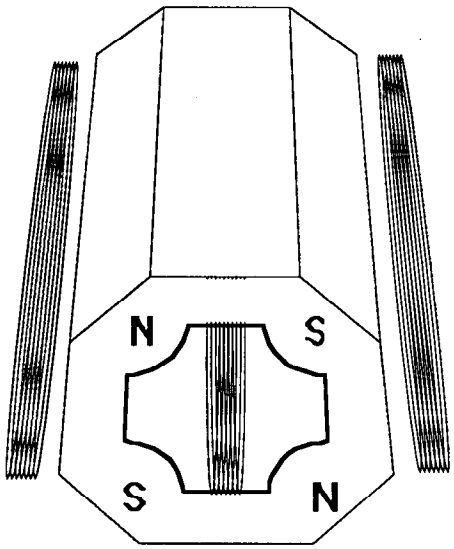

Figure 5. Schematic of an inertially suspended pickup coil in a FF quad with an exterior corrector coil.

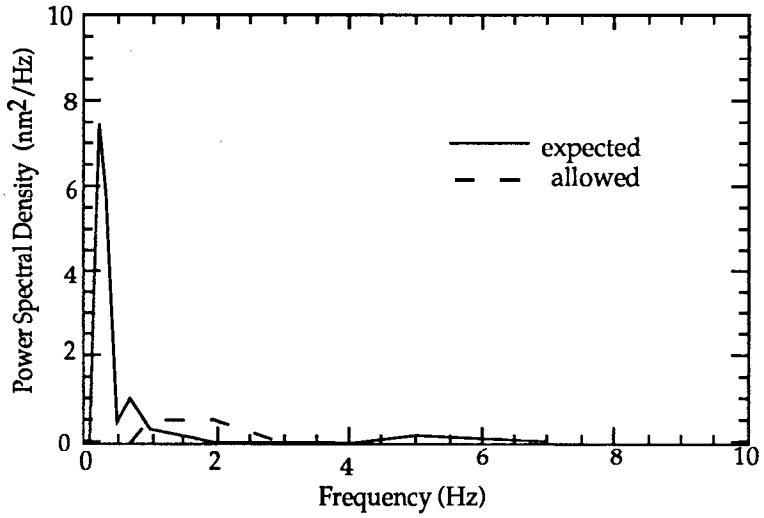

Figure 6. Net result of vibrational noise, magnet support, and fast feedback and magnetic stabilization.

proof of principle experiment using a pneumatic isolator from Newport Equipment Co. and a short piece of permanent quad magnet graciously lent to us by Cornell University.

In sum, if we take the vibration expected from ground motion, the effects of the support tube, the suppression from a second order deadbeat fast feedback correction and the local magnetic stabilization into account we are left with residual vibration as presented in Fig. 6, where the vertical axis is power spectral density in nm^2/Hz. The dashed line presents an arbitrary area of 1 nm^2 for comparison. The conclusion of these studies to date is that, while the problem is not yet solved, the seemingly hopeless task of achieving 1 nm beam stabilization at the final focus is within an order of magnitude of being solved.

4. Synchrotron Radiation Backgrounds

While a great deal of effort is being expended to make sure that the newer backgrounds from beam-beam interactions do not swamp the detector, it seems prudent to revisit the synchrotron radiation (SR) background source, considering it at the maximum NLC energy of 1 TeV. The problem is attacked in two steps.

To begin, SR photons are generated using the program QSRAD[5] developed for PEP. Input parameters include: the last 200 m of the NLC beamline[6] with the locations and bending strengths of the last 5 quads Q1–Q5; their apertures, notably that of the final quad Q1: r = 3.3 mm and 1.5 m < z < 4.2 m; and the *assumed* beam intensity distribution.

The program traces a 1 sigma reference ray at angular divergence $\theta^*_x = \theta^*_y =$ 22.4 μrad from the IP to a point upstream of Q5. This reference ray is used to construct rays on a grid of dimensions $\pm n\sigma_x$ and $\pm n\sigma_y$. These rays are then transported back downstream to the IP, the SR from each magnet calculated and projected onto the apertures and weighted by the beam intensity distribution. Two cases for collimation are considered: n=10 and n=8.

The results of this part of the calculation are roughly summarized in Fig. 7. Given the sets of apertures currently used, only the photons resulting from vertical bending contribute. As a Gaussian beam with $\theta^*_x = \theta^*_y = 22.4$ μrad will cause no detector hits at all, this calculation depends critically on the assumed beam tail. Here we take it to be flat and to contain 1% of the beam. Thus the final numbers will be due to two 500 GeV beams, each with 10^{12} particles and 10^{10} particles in a flat tail.

In the next step, the three sources of photons striking Q1 are propagated into a prototype NLC detector using EGS. To account for the ±20 mrad crossing angle, this is done in two steps. First, we record the position and momenta of all particles produced by the photons interacting on Q1 that cross a plane at the IP side of Q1 at z = 1.5 m and inside r = 20 cm. There are about 90k particles, 89% of which are photons, crossing this plane; most are due to the highest energy photons striking a glancing blow at the tip of Q1. Next, these particles are rotated and offset to account for the crossing angle and again propagated with EGS into the IR region where, after multiple interactions on the IR masks, they enter the vertex detector (VXD) and central drift chamber (CDC).

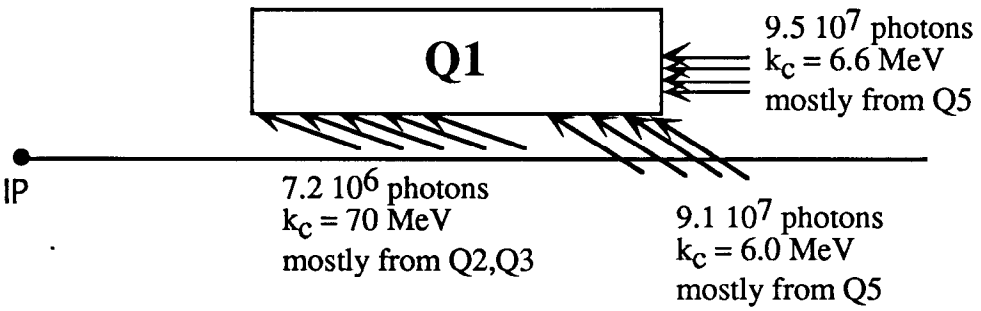

Figure 7. SR photon distribution input to EGS simulation of detector. Critical energies are given for reference, but the EGS input includes the energy spectrum.

Small radius VXD		#photons / train	$\#e^{\pm}$ / train	$\#e^{\pm}$ / mm^2/train
VXD-L1	(1.4 cm)	2.28E+04	7.92E+04	27.2
VXD-L6	(4.0 cm)	1.56E+05	4.48E+05	18.6
CDC	(25 cm)	2.62E+06	1.54E+04	
Larger Radius VXD				
VXD-L1	(6.0 cm)	2.36E+05	2.00E+05	3.32
VXD-L6	(20 cm)	6.11E+05	7.00E+03	0.1
CDC	(25 cm)	1.77E+06	1.40E+03	

Table 1. Photon and electron hits on an NLC VXD and CDC from SR photons due to beam tails collimated at 10σ.

Two NLC proto-detectors are considered. The first is composed of a six-layer CCD-based vertex detector covering $\pm 53^{o}$ in polar angle and located in radius from 1.4 to 4.0 cm; it is complemented by an SLD-like central drift chamber (CDC) with an inner radius of 25 cm. In the second case, the VXD spans the radius from 6.0 to 20 cm. Both assume a 2 Tesla solenoidal field. Electrons and photons that cross each layer of the VXD and CDC inner wall are counted in both the 10σ and 8σ cases. These results are summarized for the 10σ case in Table 1. The mean photon energy is around 2 MeV, while the mean electron energy is around 20 MeV.

To interpret these numbers consider the following. Photons crossing the VXD have, according to EGS, not interacted. Only electron hits are responsible for backgrounds. The density of these hits, as tabulated in the last column of Table 1, are what is important. It is considered[7] that a density of 10 hits/mm^2/train crossing would cause sufficient confusion in the tracking to create a problem. For reference, consider that in the SLD CCD-based vertex detector, 20 hits/mm^2/train crossing would correspond to a 1% occupancy; typical occupancy is 10^{-4}. There is a factor of 10 reduction in hit density in going from the small radius VXD to the larger at the inner layer; this increases to a factor of 200 for the outermost layer of the VXD. We have not yet considered the interaction probability or effect of the large numbers of photons and electrons emanating from the CDC inner wall.

It is clear that the edge of the 10σ beam tail is causing SR photons to strike the tip of Q1 thus causing the relatively large backgrounds listed in Table 1. When we consider the 8σ case, we find that the hit density in the case of the large radius VXD falls to 2E-3 at L1 and 4E-4 at L6. Collimation at this level will be required to provide good security against SR backgrounds.

For comparison, the same EGS simulation has been used to find the backgrounds associated with tracks emanating from beam-beam interactions as simulated by ABEL. Note that here we have only done the simulation for 250 GeV beams. Table 2 indicates the number of photon and electron hits. It appears, comparing this 250 GeV simulation to the SR calculation at 500 GeV and 10σ collimation, that the beam-beam problem is relatively less important.

Small radius VXD		**#photons / train**	**#$e^{\pm}$ / train**	**#$e^{\pm}$ / mm^2/train**
VXD-L1	(1.4 cm)	200	6200	1.98
VXD-L6	(4.0 cm)	0	800	0.34
CDC	(25 cm)	4.2E+04	200	
Larger Radius VXD				
VXD-L1	(6.0 cm)	200	200	0.002
VXD-L6	(20 cm)	1000	0	0
CDC	(25 cm)	4200	0	

Table 2. Beam-Beam induced photon and electrons crossing an NLC VXD and CDC for a 250 GeV ABEL simulation

The reader is cautioned that this is very much work in progress. More systematic SR calculations as a function of collimator setting are required. In particular, we need to investigate tails in y out to much larger than 10σ. More work is required to directly compare these results with the ABEL code, and more work is required to make sure we understand photon and electron interactions in the drift chamber.

5. Muon backgrounds

The generation of muon backgrounds in the detector by the production of Bethe-Heitler pairs in the collimator sections of the NLC has been reported previously.[8] More recent work, incorporating positron annihiliation graphs as well, has been done to better understand their origins and to devise ways of minimizing its effect at the detector. Essentially, this means finding the optimum placement and shape for toroidal field muon spoiler magnets in the area downstream of the collimation section. Figure 8 shows a layout of the last section of the NLC beamline. The current estimate for the optimal position of the toroids and locations of the collimators causing muons are indicated. With the spoilers as shown, only muons of energy greater than 300 GeV reach the detector.

Figure 9 indicates the improvement to be had by instrumenting the tunnel with spoilers. It shows the number of electrons lost on a given collimator required to produce one muon that finds its way into the detector. With the spoilers, $\approx 10^{10}$ electrons are required to produce a single muon. Recall that this is consistent with the numbers we have been assuming for flat tail backgrounds: 1% of a 10^{12} particle bunch train. Without the spoilers, the same 10^{10} particles scraped on the first collimator at 7400 ft from the IP will produce 25 muons, while, were they to be scraped on the last collimator at 4500 ft, 250 muons would result.

We find that it is best to fill the tunnel completely: round toroids in a rectangular tunnel do not work well. If a 10' x 10', rather than a 7.5' x 7.5', tunnel is used in the simulation, 5–10 times as many muons result, unless the larger tunnel cross section is also completely filled by the spoilers. Removing the big bend makes backgrounds about 10 times worse. The assumed detector cross section is 6 x 6 m^2; typically 5–10 times as many muons reach the IR, but miss the detector.

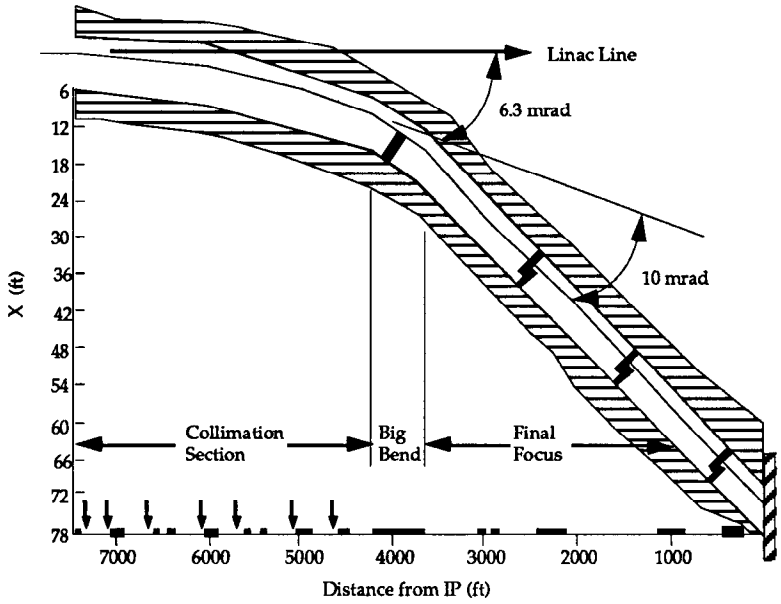

Figure 8. Layout of collimators and muon spoilers in the NLC. Collimator positions and magnetic components are indicated by arrows or by blocks, respectively, on the x axis. Spoilers location in the tunnel and the detector at the IP are shown .

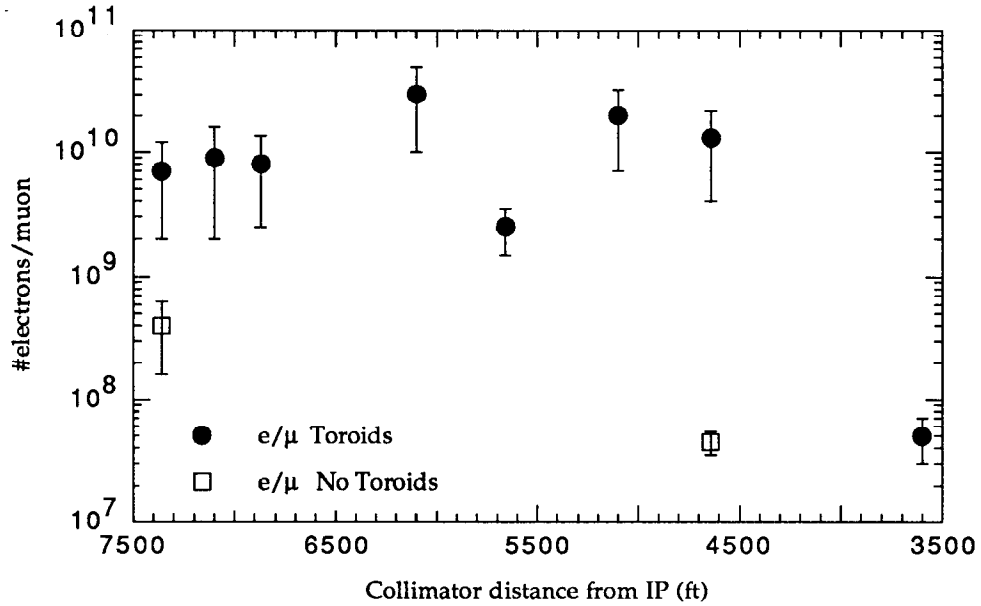

Figure 9. Number of 500 GeV positrons scraped on a given collimator to produce 1 muon in the detector.

6. References

1. C. Adlolphsen, W. Ash, T. Barklow, G. Bowden, D. Burke, C. Field, S. Hertzbach (University of Massacheusetts), M. Hildreth, J. Hodgson, J. Irwin, L. Keller, R. Kofler (University of Massacheusetts), T. Markiewicz, A. Odian, G. Punkar, M. Ronan (LBL), and S. Smith.
2. See for example R.Ruth, in *Proceedings of the 1990 DPF Summer Study on High Energy Physics: Research Directions for the Decade, Snowmass, CO, June 25–July 13, 1990* (SLAC–PUB–5597).
3. M. Ronan, in *Proceedings of the 2nd International Workshop on Physics and Experiments With Linear e^+e^- Colliders, Waikoloa, HI April 26–30, 1993*..
4. T. Himel *et al*, in *Proceedings of 8th Real - Time Computer Application in Nuclear, Particle, and Plasma Physics,* Vancouver, Canada, 8–11 June 1993 (SLAC–PUB–6246).
5. H. deStaebler and S. Hertzbach, private communication.
6. R. Helms, NLC beamline layout, using TRANSPORT TLCFF_5, June 1992.
7. C. Damerell, in *Proceedings of the 2nd International Workshop on Physics and Experiments With Linear e^+e^- Colliders, Waikoloa, Hil April 26–30, 1993.*
8. L.P. Keller, in *Proceedings of the 1990 DPF Summer Study on High Energy Physics: Research Directions for the Decade, Snowmass, CO, June 25–July 13, 1990* (SLAC–PUB–5652).